LANGMUIR

Interfaces: Adsorption, Reactions, Films, Forces, Measurement Techniques, Charge Transfer, Electrochemistry, Electrocatalysis, Energy Production and Storage

Pd nanoparticles confined in the porous Graphene-like carbon nanosheets for olefin hydrogenation

Zhe Chen, Weixue Wang, Yifei Zhang, Yu Liang, Zhi-Min Cui, and Xiangke Wang

Langmuir, **Just Accepted Manuscript** • DOI: 10.1021/acs.langmuir.8b02785 • Publication Date (Web): 29 Sep 2018

Pd nanoparticles confined in the porous Graphene-like carbon nanosheets for olefin hydrogenation

Zhe Chen,[a] Weixue Wang,[a] Yifei Zhang,[a] Yu Liang,[a] Zhimin Cui [,b] and Xiangke Wang [*, a]*

[a] College of Environmental Science and Engineering, North China Electric Power University, Beijing, 102206, PR China

[b] School of Chemistry, Beihang University, Beijing 100191, PR China

KEYWORDS: Palladium, confined, porous graphene, hydrogenation, catalysis

ABSTRACT: As a novel type of defective graphene, porous graphene has been considered an excellent support material for metal clusters, as the interaction between defective carbon atoms surrounding with the metal NPs is very different from that on ordinary supported catalyst. In this work, we reported a facile three-step method to confine the Pd NPs and grow the graphene-like carbon nanosheets (GLCs) in the same interlayer space of layered silicate, generating embedded Pd NPs in the pores of porous GLCs in situ. The Pd@GLCs nanocomposite not only exhibited highly active activity and stability than common commercial Pd/C catalyst for the hydrogenation of olefins, but also superior ability of resisting high temperature, which benefitted from the two dimensional structure of layered GLCs, the confinement of Pd and the increased edge and defect of the unsaturated carbon atoms in GLCs.

Introduction

Supported metal nanoparticles (NPs) are the most widely investigated heterogeneous catalysts in catalysis community. The interaction between the metal and support materials have great influence on the stability and adsorption properties of catalysts, which lead to different activity and selectivity.[1-4] Among the common catalyst supports, carbon materials, such as active carbon, graphene and carbon nanotubes (CNTs) are widely employed as support due to their high surface areas, excellent structure stability, and non-toxicity.[5-9] However, the migration, agglomeration, and sintering of metal NPs on the surface of pristine graphene (or CNTs, etc.) are always unavoidable because the functional groups as the anchoring sites are absent on the carbon support.[10,11] How to solve this problem becomes a significant topic of the catalyst design based on carbon materials.[12] Take graphene as an example, many approaches have been proposed to improve the interaction of metal NPs and carbon support, such as by introducing oxygen or nitrogen-containing groups, doping heteroatom on graphene, and fabricating pores with defective sites on the graphene.[13-20]

As a novel type of defective graphene, porous graphene has been considered an excellent support material for metal clusters, as the interaction between defective carbon atoms surroundings with the metal NPs is very different from that on ordinary supported catalyst.[21,22] Banhart et.al demonstrated that defects in graphene and CNTs could trap metal atom and prevent it from diffusing effectively,[23] thus improving the stability of the composite as a catalyst. Not just in regard to the stability, the electron character of metal also might be influenced a lot when metal clusters were embedded in the porous graphene, which was revealed by theoretical calculations research particularly. Wang et.al investigated electronic structures of metal clusters (Pd, Ir, and Rh) supported on pristine graphene and porous graphene with density functional

theory (DFT) calculations, and reported that graphene with nanopores could stabilize the metal clusters, downshift the d-band center of the metal clusters and change the binding energy of reagents substantially.[24]

What's more, the porous graphene itself exhibit special electron or adsorption properties due to the abundant defective carbon atoms along the pores. For example, several works proved that the reaction rate of methane decomposition catalyzed by defective carbon materials was linearly dependent on the number of -CH=CH- defective sites.[25,26] In brief, as the support of catalyst, the enriched unsaturated carbon atoms on porous graphene will bring significant effect to the catalyst' performance.

Although several exciting theoretical reports have proved the significant impact of porous graphene on catalysis, the related experimental studies are limited. The severe mismatches may derive from the difficulty to synthesize porous graphene with subnano-sized pores,[23,27] as well as the difficulty of the precise control to embed all the metal NPs into the pores on porous graphene perfectly.

Herein, we reported a facile three-step method to confine the Pd NPs and grow the graphene-like carbon nanosheets (GLCs) in the same interlayer space of layered silicate, generating embedded Pd NPs in the pores of porous GLCs in situ. The Pd@GLCs nanocomposite not only exhibited highly active activity and stability than common commercial Pd/C catalyst for the hydrogenation of olefins, but also superior ability of resisting high temperature. The two-dimensional structure of layered GLCs and the intimate contact between the confined Pd and GLCs was supposed to account for the superior performance of the Pd@GLCs nanocomposite.

Experimental Methods

Synthesis of RUB-15 nanoplates

In a typical process, 17.78 g TMAOH (Tetramethylammonium hydroxide, 25 wt% solution) was mixed with 12.22 g TEOS (Tetraethyl orthosilicate) at room temperature under stirring. After stirred overnight, the solution was transferred to a 50 mL Teflon-lined autoclave, which next would be kept in the oven at the temperature of 140 ˚C for 7 days. Lastly, the product was collected by filtration and washed with acetone till the pH decreased to 7, and then dried at 60 ◦C.

Synthesis of Pd@GLCs

100 mg RUB-15 was dispersed in 50mL distilled water and stirred for 20 min. At the same time, 0.1 g $SnCl_2$ was dissolved in 20 mL 0.02 M HCl solution. Then the $SnCl_2$ solution was added into RUB-15 suspension under stirring for 10 min. Afterwards the suspension was centrifuged and washing with distilled water for five times. The precipitate was dispersed in 50 mL distilled water, and mixed with 500 μL $PdCl_2$ (0.0564 mol/L) solution. Ten min later, 10 mL of 0.15 mol/L NaCOOH solution was added following stirring for 5 h. After centrifugation and washing with distilled water five times, the precipitate Pd/RUB-15 was obtained and dried at 60 ºC for 12 h.

100 mg Pd/RUB-15 and 150 mg of glucose were dispersed in 5mL of distilled water and stirred overnight. Then, 30 μL of concentrated sulfuric acid was added. Afterward, the mixture was stirred for another 10 min and heated at 110 °C for 10 h. The black product was collected carefully and calcined at 900 °C in Ar flow for 4 h (rate: 5 °C/min) to remove oxygen and organic species and improve the graphitization of GLCs. Then, the graphitized Pd@GLCs-RUB-15 was stirred with 5 mol/L NaOH solution tenderly for 12 h. After the etching of RUB-15, the Pd@GLCs was harvested.

Olefin hydrogenation

A 25 mL steel autoclave was charged with Pd@GLCs (4.6 wt%, 5 mg), an olefin (2.5 mmol), 1,3,5-trimethylbenzene (internal standard, 285 mL, 2.0 mmol) and 5 mL ethanol. The autoclave was evacuated and backfilled with H_2 (3 cycles, 1.0 MPa). Then, the mixture was stirred in a 25 °C water bath under 1.0 MPa H_2 atmosphere for the desired time. Gas chromatograph (Shimadzu GC-2010Plus) equipped with a flame ionization detector (FID) and a Rtx-5 capillary column (0.25 mm in diameter, 30 m in length) was used to analyzed the yield of product, and the product identity was ascertained by GC-MS (Shimadzu GCMS-QP2010S). The commercial Pd/C catalyst (5 wt%) was purchased in Sigma-Aldrich.

Characterization

The crystal structure of the Pd@GLCs was characterized using an X-ray diffraction meter (XRD-Rigaku) with Cu Kα radiation (λ = 1.54 Å). Scanning electron microscopy (operated on JEOL JSM-7800F), transmission electron microscope, high resolution TEM images and energy dispersive absorption X-ray (EDAX) spectroscopy (operated on JEM-ARM200F) was used to examine the size and morphology of RUB-15 and Pd@GLCs. The concentrations of Pd^{2+} loss in the reaction were analyzed using inductively coupled plasma atomic emission spectroscopy (ICP-AES; Shimadzu ICPE-9000). The X-ray photoelectron spectroscopy (XPS) spectra was performed on Thermo VG RSCAKAB 250X with VG SCIENTA KKLaser.

Results and discussion

The Pd@GLCs composite was fabricated in a three-step in situ carbonization method in the interlayer space of layered silicate as shown in Scheme 1. The layered silicate RUB-15 was a layered silicate ($[N(CH_3)_4]_8[Si_{24}O_{52}(OH)_4]\cdot 20H_2O$) with side length of 5−10 μm and thickness of 100 nm approximately (Figure S1). [28] In the structure of RUB-15, the Tetramethylammonium (TMA) cations as well as water molecules were filled in the hemihedral cavities inside the

interlayer, which stabilized the layered structure. With the basal d spacing of 1.4 nm, the ion-exchange between TMA^+ inside the layered silicate RUB-15 and other metal cations was feasible. In this synthesis route, the $SnCl_2$ solution was added into RUB-15 suspension, as the ion-exchange between TMA^+ and Sn^{2+} took place. Then Sn^{2+} could act as the reductive site for $PdCl_4^{2-}$, which assured that all the Pd NPs were loaded inside the interlayer of RUB-15. Afterwards, the glucose was intercalated in the interlamellar space of RUB-15 and then the carbon nanosheets were generated from the carbonization of glucose. At last, the Pd@GLCs nanocomposite was obtained after the graphitization of carbon nanosheets and the removal of RUB-15.

Scheme 1 The preparation of Pd@GLCs composite in three steps.

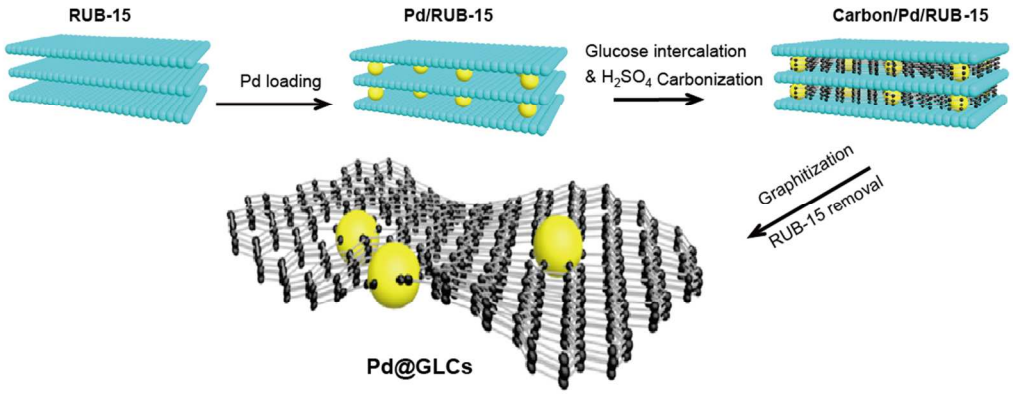

As shown in Figure 1, the uniform Pd nanoparticles with particle size of 5±2 nm were successfully obtained on the GLCs without any agglomeration. The average size of Pd nanoparticles was found to be 4.5 nm inspired by the size distribution (inset of Figure 1c). From the SEM image (Figure 1a) and TEM images (Figure 1b-c) of Pd@GLCs, the GLCs looked like monolayer-patched graphene and quite a number of GLCs were exfoliated as single or few-layers graphene. The Pd NPs were located and confined in the pores of GLCs, as obvious vacant regions existed around Pd NPs (Figure 1c). It was believed that the confined structure endowed

Pd superior stability and efficient electron/ions transport on the GLCs. Figure 1d was the HRTEM of a selected section Pd NPs. The lattice fringes of (111) planes with a d spacing of 0.225 nm indicated good crystallization of Pd nanoparticles. From the ICP-AES analysis, the Pd content in the Pd@GLCs was calculated to be 4.6 wt%. Energy dispersive spectroscopy (EDS) mapping of Pd@GLCs using STEM (Figure 1e) revealed the homogeneous and highly-uniform distribution of Pd NPs on the Pd@GLCs.

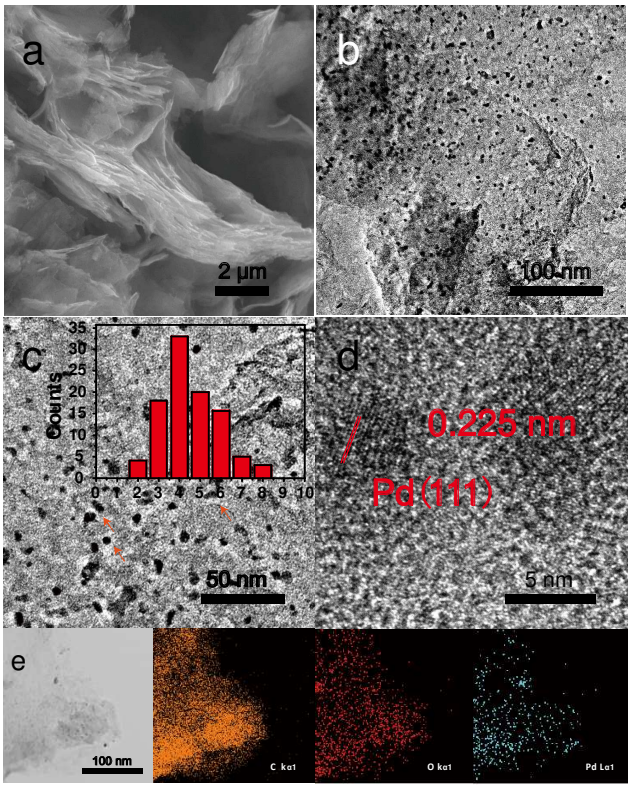

Figure 1 (a) The SEM image, (b-c) TEM images, (d) HRTEM images and (e) compositional EDS mapping of Pd@GLCs composite.

Figure 2a displayed the XRD pattern of the Pd@GLCs composite. The wide peaks around 25.0 degree and the weak peak at 44.8 degree were attributed to the GLCs. No peaks belong to Pd were observed at XRD patterns, which might due to the ultra-small size of the Pd NPs. He et.al also reported the absence of Pt-phase diffraction peak of Pt/TiO_2 in their XRD patterns, and

attributed it to the strong metal interaction between the Pt and the TiO_2 support.[29] Control experiments were carried out by preparation of GLCs that intercalated in RUB-15 first and then loading Pd NPs on the GLCs afterwards (denoted as Pd@out-GLCs). The XRD patterns of Pd@out-GLCs composite showed the apparent peak at 39.6 degree which was well assigned to Pd (111) plane (Figure S2). The difference of the XRD patterns between the Pd@GLCs and Pd@out-GLCs further proved that there was strong interaction between Pd and GLCs in the Pd@GLCs composite. The Raman spectra of Pd@GLCs (Figure 2b) showed the disordered band at~1356 cm^{-1} (D-band), the graphitic band at ~1587 cm^{-1} (G-band), and a wide 2D-band around 2870 cm^{-1}. The measured intensity I_D/I_G ratio is about 0.735. The low intensity ratio of I_D/I_G suggested that the sp^2 carbon atoms domain and the GLCs was largely graphitized.[30]

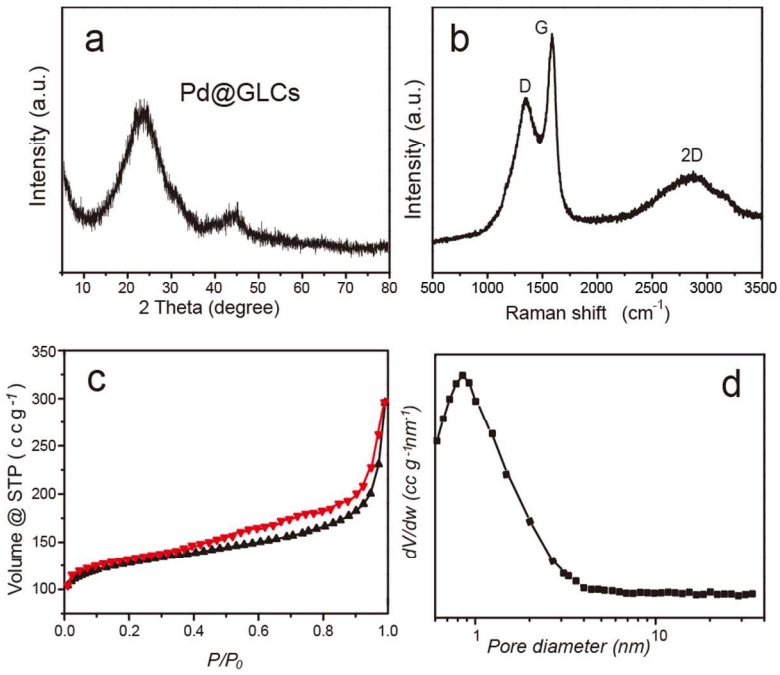

Figure 2 (a) The XRD patterns (b) Raman spectra of Pd@GLCs (c) The N_2 adsorption–desorption curve of Pd@GLCs (d) The pore distribution of the Pd@GLCs based on NLDFT method.

Figure 2c revealed the N_2 adsorption–desorption curve of Pd@GLCs and it belonged to type-IV isotherm according to IUPAC classification. The Brunauer– Emmett–Teller (BET) surface area was calculated as 517.6 m^2 g^{-1}. The relatively large surface area indicated that the obtained GLCs has sufficient diffusion paths for mass transfer and abundant active sites to combine reagents. At the same time, the pore diameter of the GLCs based on Nonlocal density functional theory (NLDFT) method is∼1 nm (Figure 2d), which were consisted with the fact that interlayer spacing of the GLCs was caused by the removal of layered silicate RUB-15. The two-dimensional Pd@GLCs structure and the ∼1 nm spacing ensured mass-transfer rates and high catalytic permeation for species involved in the catalysis.

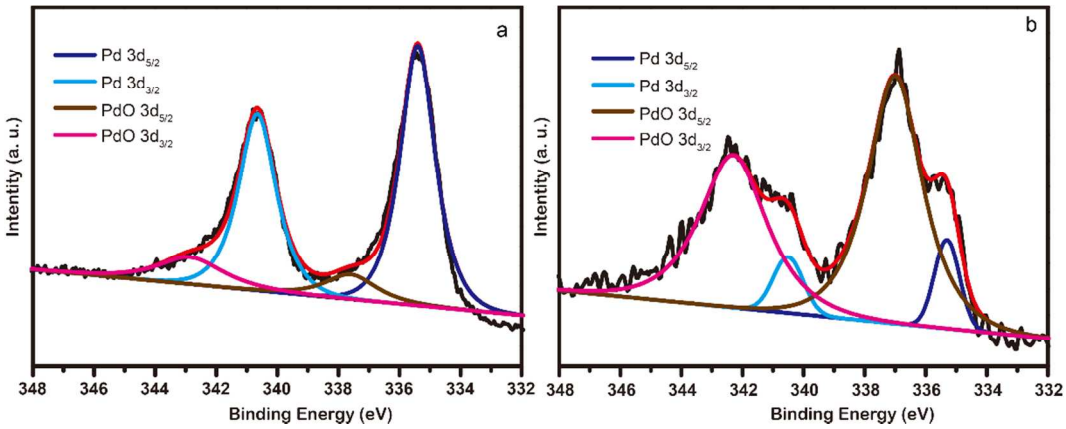

Figure 3 The XPS survey spectrum of Pd 3d in (a) Pd@GLCs composite and (b) commercial Pd/C catalyst.

The XPS spectrum of Pd 3d was shown in Figure 3. The spectrum of Pd 3d could be deconvoluted into four single peaks in both Pd@GLCs composite and commercial Pd/C catalyst (Figure 3). The peaks at 335.4 eV and 340.6 eV were assigned to Pd (0), and the other two peaks at 337.2 eV and 342.3 eV were the characteristic peaks of Pd (II) due to the partially oxided Pd[31,32]. The intensity of Pd (II) in Pd@GLCs composite was much weaker than that of

commercial Pd/C, indicating that there was strong interaction between the Pd nanoparticles and the GLCs, which further protected the Pd nanoparticles from oxidation.

The hydrogenation of styrene was chosen as a model reaction to evaluate the catalytic performance of the Pd@GLCs composite under 1 MPa hydrogen pressure and at room temperature. It is observed that the as-prepared Pd@GLCs exhibited outstanding catalytic performance for the hydrogenation of various kinds of olefins, as shown in Table 1. The conversion of styrene, 4-methylstyrene, 4-chlorostyrene and 4-methoxystyrene achieved almost 100 % in 15 minutes (Table 1, entry 1-4), giving the corresponding hydrogenated products that be confirmed by GC and GC-MS. The turnover frequency (TOF) quantifies the specific activity of a catalytic centre by the number of molecular reactions occurring at the centre per unit time. The turnover frequency (TOF) was calculated to be 21284 h^{-1} for entry 1-4. The olefins conversion in Entry 5 indicated that the hydrogenation rate of cyclohexene was slower than that of styrene (Table 1, entry 5). The relatively inert reactivity of cyclohexene and its larger tri-dimensional size might attribute to the lower reaction rate (entry 5). According to the TOF value, the catalytic performance of Pd@GLCs was better than reported Pd catalyst, such as Pd@Fe@meso-SiO_2 composite[33] (TOF=7918 h^{-1} for styrene hydrogenation) and the commercial Pd/C in this work (TOF=16180 h^{-1}) at same experiment condition. In addition, the selectivity of all the reagents was nearly 100%, as no by-product was detected in GC-MS.

Table 1 Olefin hydrogenation catalyzed by Pd@GLCs

Run	Olefin	Product	Time (min)	Conversion (%)	TOF (h^{-1})
1			15	> 99	2.1×10^5
2			15	> 99	2.1×10^5
3			15	> 99	2.1×10^5
4			15	> 99	2.1×10^5
5			60	> 99	5.3×10^4
6			30	> 99	1.0×10^5

Reaction conditions: Olefin (2.5 mmol), Pd @GLCs (5 mg), EtOH (5 mL), 25 °C, under 1.0 MPa H_2 atmosphere. [b] The conversion of reagents was determined by GC, and the identity of the product was ascertained by GC-MS.

Stability is another important parameter for a heterogeneous catalyst. Figure 4a displayed the conversion of styrene at 15 minutes catalyzed by Pd@GLCs and commercial Pd/C in cycling tests of styrene hydrogenation. Note that the amount of Pd in Pd@GLCs and commercial Pd/C was kept to be equal. It can be found that the activity of fresh Pd/C was comparable with fresh

Pd@GLCs, and 76% conversion was achieved at 15 minutes catalyzed by Pd/C. However, the conversion of styrene catalysed by commercial Pd/C decreased significantly in the followed reaction runs, and the conversion dropped to about 32% in the 8th runs. In sharp contrast, the Pd@GLCs composite showed much better stability in the consecutive reaction runs. The conversion of styrene still maintained higher than 90 % after eight reaction cycles. In addition, the concentration of Pd in the supernatant of the hydrogenation reaction system catalyzed by Pd@GLCs and commercial Pd/C after the reaction was measured by ICP-AES, and it was found the concentration of Pd was around 316 ppb and 20 ppb in the Pd/C and Pd@GLCs systems, respectively, indicating that the leaching Pd could be much reduced by the confinement of Pd NPs in the porous GLCs.

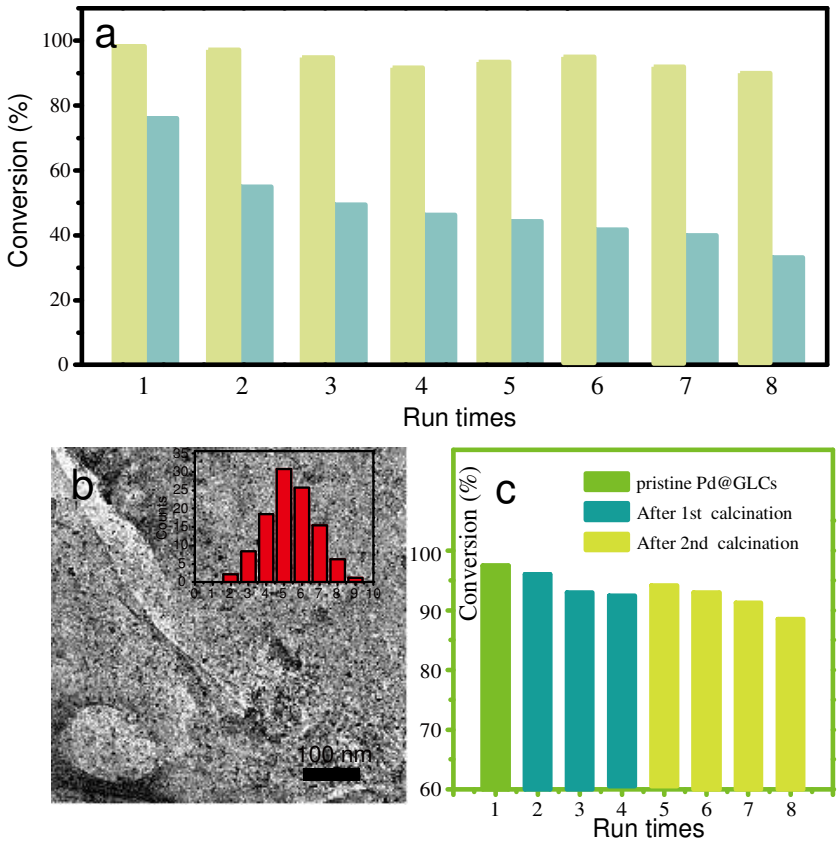

Figure 4 (a) The cycling performance of the Pd@GLCs (yellow columns) and commercial Pd/C (blue columns) catalyst catalyzed styrene hydrogenation as a model reaction. (b) The TEM image and the size distribution of Pd@GLCs after calcination for two times. (c) The catalytic activity of Pd@GLCs in the designed cycle experiment.

It was known that the surface restructuring and sintering of Pd nanoparticles was prone to occurring after annealing even at relatively low temperature (above 400 °C) on support, either on silica, alumina or graphene.[34,35] Supported metal nanoparticles, especially for noble metal NPs, showed rapid growth if the reaction temperature was very high. We further investigated the ability of resisting high temperature of Pd@GLCs. In this work, the Pd@GLCs was fabricated by carbonization at 900 °C for 4 hours under nitrogen atmosphere, thus the Pd@GLCs was speculated to possess superior thermal stability. In a designed experiment, the fresh Pd@GLCs was used as catalyst for hydrogenation of styrene once, then calcined at 900 °C for 1 hours under Ar atmosphere and worked for three times. Next, the Pd@GLCs was calcined for the second time, and used as catalyst for the following four catalytic reaction. Figure 3b displayed the TEM image of the final Pd@GLCs after calcination at 900 °C for two times. No obvious change of Pd NPs (sintering or grownup) could be found on the calcined Pd@GLCs. The diameter of Pd NPs still kept at 5±2 nm, and the average size was calculated to be 5.3 nm by the size distribution. The Figure 3c showed the catalytic performance of fresh and calcined Pd@GLCs in eight consecutive hydrogenation of styrene reaction. The conversion of styrene catalyzed by fresh Pd@GLCs was 98.2 %, whereas the conversion of styrene was still higher than 88.7% with the calcined Pd@GLCs catalyst in the 8th reaction runs. The superb ability of resisting high temperature was closely related with the structure of the Pd@GLCs composite. The confinement

of the porous GLCs could prevent the Pd NPs from shifting and agglomeration on the surface of GLCs, and thus help to maintain their high catalytic activity.

The high catalytic activity and superb stability of the Pd@GLCs were attributed to the specific formation process and structure of the final product with Pd NPs embedded in the graphene-like carbon. (1) the specific structure that Pd NPs embedded in the GLCs endowed it with outstanding activity and stability. Lee reported that the edges of graphene layers were the activated chemisorption sites in the hydrogenation of acetylene.[36] The dramatically increased edge and defects of GLCs layers could adsorb the olefins reagents. The GLCs with nanopores exhibited stronger binding energies than pristine graphene, and the interactions of graphene with nanopores and confined Pd NPs were better comparing with the supported metal cluster on pristine graphene. The intimate contact between GLCs and Pd impacted on the properties of Pd NPs and promoted the catalytic reaction a lot. (2) The unsaturated carbon atoms exhibited act as anchor sites to immobilize Pd nanoparticles, which efficiently prevents the Pd NPs aggregation and leaching. The porous graphene confined the Pd NPs strongly like a pliers, assuring the cycling and stability of Pd@GLCs. (3) the graphene-like carbon nanosheets generated in the layered silicate had relatively large surface area. The measured BET surface area of Pd@GLCs composite was 517.6 m^2/g. The large surface area and hydrophobic nature of the GLCs would adsorb H_2 and olefins, facilitating the effective contact between reagents and the spread out of the products.

Conclusions

In summary, the Pd@GLCs composite with the structure that Pd NPs embedded in the pores of porous GLCs were fabricated by growth and graphitization of carbon source around Pd NPs in the interlamellar space of layered silicate. The Pd@GLCs composite exhibited not only high

activity to the hydrogenation of olefins, but also superb stability. The conversion of styrene in the hydrogenation reaction maintained higher than 91.7% even after calcination of Pd@GLCs at 900 °C for 2 times in the 8th reaction cycle, which was much better than the commercial Pd/C. The superior catalytic performance of the Pd@GLCs was benefited from their specific structure. The increased edge and defect of GLCs layers provided more adsorption sites for reagents, while the interaction between Pd NPs and GLCs enhanced the activity, and the confinement of Pd NPs by the GLCs much increased their catalytic stability.

Supporting Information

The Supporting Information is available free of charge on the ACS Publications website at DOI: Details on the SEM and TEM images of RUB-15, the XRD patterns of Pd@out-GLCs, and the N_2 adsorption−desorption curve of Pd@GLCs..

AUTHOR INFORMATION

Corresponding Author

* Email: xkwang@ncepu.edu.cn

cuizhm@buaa.edu.cn

Notes

The authors declare no competing financial interest.

ACKNOWLEDGMENT

The authors gratefully acknowledge financial support from National Natural Science Foundation of China (NSFC 51502089, 51772010) and the National Key Research and Development Program of China (2017YFA0207002).

ABBREVIATIONS

GLCs, graphene-like carbon nanosheets.

REFERENCES

(1) Qiao, B. T.; Wang, A. Q.; Yang, X. F.; Allard, L. F.; Jiang, Z.; Cui, Y. T.; Liu, J. Y.; Li, J.; Zhang, T. Single-atom catalysis of CO oxidation using Pt-1/FeOx. *Nature Chemistry* **2011**, *3*, 634-641.

(2) Liang, Y.; Chen, Z.; Yao, W.; Wang, P. Y.; Yu, S. J.; Wang, X. K. Decorating of Ag and CuO on Cu Nanoparticles for Enhanced High Catalytic Activity to the Degradation of Organic Pollutants. *Langmuir* **2017**, *33*, 7606-7614.

(3) Zhao, M. T.; Yuan, K.; Wang, Y.; Li, G. D.; Guo, J.; Gu, L.; Hu, W. P.; Zhao, H. J.; Tang, Z. Y. Metal-organic frameworks as selectivity regulators for hydrogenation reactions. *Nature* **2016**, *539*, 76-80.

(4) Zhao, M. T.; Deng, K.; He, L. C.; Liu, Y.; Li, G. D.; Zhao, H. J.; Tang, Z. Y. Core-Shell Palladium Nanoparticle@Metal-Organic Frameworks as Multifunctional Catalysts for Cascade Reactions. *Journal of the American Chemical Society* **2014**, *136*, 1738-1741.

(5) Bonarowska, M.; Rarog-Pilecka, W.; Karpinski, Z. The use of active carbon pretreated at 2173K as a support for palladium catalysts for hydrodechlorination reactions. *Catalysis Today* **2011**, *169*, 223-231.

(6) Chen, Z.; Lu, J. F.; Ai, Y. J.; Ji, Y. F.; Adschiri, T.; Wan, L. J. Ruthenium/Graphene-like Layered Carbon Composite as an Efficient Hydrogen Evolution Reaction Electrocatalyst. *Acs Applied Materials & Interfaces* **2016**, *8*, 35132-35137.

(7) Siamaki, A. R.; Khder, A. E. S.; Abdelsayed, V.; El-Shall, M. S.; Gupton, B. F. Microwave-assisted synthesis of palladium nanoparticles supported on graphene: A highly active

and recyclable catalyst for carbon-carbon cross-coupling reactions. *Journal of Catalysis* **2011**, *279*, 1-11.

(8) Liu, H. Y.; Zhang, L. Y.; Wang, N.; Su, D. S. Palladium Nanoparticles Embedded in the Inner Surfaces of Carbon Nanotubes: Synthesis, Catalytic Activity, and Sinter Resistance. *Angewandte Chemie-International Edition* **2014**, *53*, 12634-12638.

(9) Jing, Y. Q.; Gui, C. X.; Qu, J.; Hao, S. M.; Wang, Q. Q.; Yu, Z. Z. Silver Silicate@Carbon Nanotube Nanocomposites for Enhanced Visible Light Photodegradation Performance. *Acs Sustainable Chemistry & Engineering* **2017**, *5*, 3641-3649.

(10) Gan, Y. J.; Sun, L. T.; Banhart, F. One- and two-dimensional diffusion of metal atoms in graphene. *Small* **2008**, *4*, 587-591.

(11) Jin, Z.; Nackashi, D.; Lu, W.; Kittrell, C.; Tour, J. M. Decoration, Migration, and Aggregation of Palladium Nanoparticles on Graphene Sheets. *Chemistry of Materials* **2010**, *22*, 5695-5699.

(12) Xi, J. B.; Sung, H. Y.; Wang, D.; Zhang, Z. Y.; Duan, X. M.; Xiao, J. W.; Xiao, F.; Liu, L. M.; Wang, S. Confined-interface-directed synthesis of Palladium single-atom catalysts on graphene/amorphous carbon. *Applied Catalysis B-Environmental* **2018**, *225*, 291-297.

(13) Li, Y. Z.; Yu, Y.; Wang, J. G.; Song, J.; Li, Q.; Dong, M. D.; Liu, C. J. CO oxidation over graphene supported palladium catalyst. *Applied Catalysis B-Environmental* **2012**, *125*, 189-196.

(14) Chen, N.; Huang, X. K.; Qu, L. T. Heteroatom substituted and decorated graphene: preparation and applications. *Physical Chemistry Chemical Physics* **2015**, *17*, 32077-32098.

(15) Liu, X.; Meng, C. G.; Han, Y. Defective Graphene Supported MPd12 (M = Fe, Co, Ni, Cu, Zn, Pd) Nanoparticles as Potential Oxygen Reduction Electrocatalysts: A First-Principles Study. *Journal of Physical Chemistry C* **2013**, *117*, 1350-1357.

(16) Su, C. L.; Acik, M.; Takai, K.; Lu, J.; Hao, S. J.; Zheng, Y.; Wu, P. P.; Bao, Q. L.; Enoki, T.; Chabal, Y. J.; Loh, K. P. Probing the catalytic activity of porous graphene oxide and the origin of this behaviour. *Nature Communications* **2012**, *3*.

(17) Xi, J. B.; Xie, C. Y.; Zhang, Y.; Wang, L.; Xiao, J.; Duan, X. M.; Ren, J. H.; Xiao, F.; Wang, S. Pd Nanoparticles Decorated N-Doped Graphene Quantum Dots@N-Doped Carbon Hollow Nanospheres with High Electrochemical Sensing Performance in Cancer Detection. *Acs Applied Materials & Interfaces* **2016**, *8*, 22563-22573.

(18) Dong, Z. P.; Le, X. D.; Liu, Y. S.; Dong, C. X.; Ma, J. T. Metal organic framework derived magnetic porous carbon composite supported gold and palladium nanoparticles as highly efficient and recyclable catalysts for reduction of 4-nitrophenol and hydrodechlorination of 4-chlorophenol. *Journal of Materials Chemistry A* **2014**, *2*, 18775-18785.

(19) Cui, X. L.; Long, Y.; Zhou, X.; Yu, G. Q.; Yang, J.; Yuan, M.; Ma, J. T.; Dong, Z. P. Pd-doped Ni nanoparticle-modified N-doped carbon nanocatalyst with high Pd atom utilization for the transfer hydrogenation of nitroarenes. *Green Chemistry* **2018**, *20*, 1121-1130.

(20) Yin, H. J.; Tang, H. J.; Wang, D.; Gao, Y.; Tang, Z. Y. Facile Synthesis of Surfactant-Free Au Cluster/Graphene Hybrids for High-Performance Oxygen Reduction Reaction. *Acs Nano* **2012**, *6*, 8288-8297.

(21) Zhang, Z. Y.; Dong, Y.; Wang, L.; Wang, S. Scalable synthesis of a Pd nanoparticle loaded hierarchically porous graphene network through multiple synergistic interactions. *Chemical Communications* **2015**, *51*, 8357-8360.

(22) Ye, R. Q.; Peng, Z. W.; Wang, T.; Xu, Y. N.; Zhang, J. B.; Li, Y. L.; Nilewski, L. G.; Lin, J.; Tour, J. M. In Situ Formation of Metal Oxide Nanocrystals Embedded in Laser-Induced Graphene. *Acs Nano* **2015**, *9*, 9244-9251.

(23) Rodriguez-Manzo, J. A.; Cretu, O.; Banhart, F. Trapping of Metal Atoms in Vacancies of Carbon Nanotubes and Graphene. *Acs Nano* **2010**, *4*, 3422-3428.

(24) Zhou, H.; Chen, X. L.; Wang, L.; Zhong, X.; Zhuang, G. L.; Li, X. N.; Mei, D. H.; Wang, J. G. Effect of graphene with nanopores on metal clusters. *Physical Chemistry Chemical Physics* **2015**, *17*, 24420-24426.

(25) Zhong, B. W.; Zhang, J.; Li, B.; Zhang, B. S.; Dai, C. L.; Sun, X. Y.; Wang, R.; Su, D. S. Insight into the mechanism of nanodiamond catalysed decomposition of methane molecules. *Physical Chemistry Chemical Physics* **2014**, *16*, 4488-4491.

(26) Huang, L. P.; Santiso, E. E.; Nardelli, M. B.; Gubbins, K. E. Catalytic role of carbons in methane decomposition for CO- and CO(2)-free hydrogen generation. *Journal of Chemical Physics* **2008**, *128*.

(27) Jang, D.; Idrobo, J. C.; Laoui, T.; Karnik, R. Water and Solute Transport Governed by Tunable Pore Size Distributions in Nanoporous Graphene Membranes. *Acs Nano* **2017**, *11*, 10042-10052.

(28) Chen, Z.; Jia, D. S.; Zhou, Y.; Hao, J.; Liang, Y.; Cui, Z. M.; Song, W. G. In situ generation of highly dispersed metal nanoparticles on two-dimensional layered SiO2 by topotactic structure conversion and their superior catalytic activity. *Applied Surface Science* **2018**, *434*, 1137-1143.

(29) Zhang, C. B.; He, H.; Tanaka, K. Catalytic performance and mechanism of a Pt/TiO2 catalyst for the oxidation of formaldehyde at room temperature. *Applied Catalysis B-Environmental* **2006**, *65*, 37-43.

(30) Li, X. H.; Kurasch, S.; Kaiser, U.; Antonietti, M. Synthesis of Monolayer-Patched Graphene from Glucose. *Angewandte Chemie-International Edition* **2012**, *51*, 9689-9692.

(31) Duan, X.; Xiao, M.; Liang, S.; Zhang, Z.; Zeng, Y.; Xi, J.; Wang, S. Ultrafine palladium nanoparticles supported on nitrogen-doped carbon microtubes as a high-performance organocatalyst. *Carbon* **2017**, *119*, 326-331.

(32) Liu, J.; Hao, J.; Hu, C.; He, B.; Xi, J.; Xiao, J.; Wang, S.; Bai, Z. Palladium Nanoparticles Anchored on Amine-Functionalized Silica Nanotubes as a Highly Effective Catalyst. *Journal of Physical Chemistry C* **2018**, *122*, 2696-2703.

(33) Yang, S. L.; Peng, L.; Cao, C. Y.; Wei, F.; Liu, J.; Zhu, Y. N.; Liu, C.; Wang, X. S.; Song, W. G. Preparation of Magnetic Tubular Nanoreactors for Highly Efficient Catalysis. *Chemistry-an Asian Journal* **2016**, *11*, 2797-2801.

(34) Cao, A.; Veser, G. Exceptional high-temperature stability through distillation-like self-stabilization in bimetallic nanoparticles. *Nature Materials* **2010**, *9*, 75-81.

(35) Zhang, Q.; Jiang, L.; Wang, H.; Liu, J. L.; Zhang, J. F.; Zheng, Y. Q.; Li, F. T.; Yao, C. X.; Hou, S. F. Hollow Graphitized Carbon Nanocage Supported Pd Catalyst with Excellent Electrocatalytic Activity for Ethanol Oxidation. *Acs Sustainable Chemistry & Engineering* **2018**, *6*, 7507-7514.

(36) Lee, S. Y.; Kwak, J. H.; Han, G. Y.; Lee, T. J.; Yoon, K. J. Characterization of active sites for methane decomposition on carbon black through acetylene chemisorption. *Carbon* **2008**, *46*, 342-348.

Table of Contents and Synopsis

The confinement of Pd and the increased edge and defect of the unsaturated carbon atoms in graphene-like carbon nanosheets endowed high efficiency on the hydrogenation of olefins and outstanding ability of resisting high temperature.